Hardware Implementation and Performance Analysis of a Current-Sensor-Free Single Cell MPPT for High Performance Vehicle Solar Arrays

Peter Wolfs
Central Queensland University
Rockhampton Mail Center, QLD 4702, Australia
Email: p.wolfs@cqu.edu.au

Quan Li
Central Queensland University
Rockhampton Mail Center, QLD 4702, Australia
Email: q.li@cqu.edu.au

***Abstract* - A Maximum Power Point Tracker has been previously developed for the single high performance triple junction solar cell for hybrid and electric vehicle applications. The Maximum Power Point Tracking (MPPT) control method is based on the Incremental Conductance (IncCond) but removes the need for current sensors. This paper presents the hardware implementation of the Maximum Power Point Tracker. Significant efforts have been made to reduce the size to 18 mm × 21 mm (0.71 in × 0.83 in) and the cost to close to $5 US. This allows the MPPT hardware to be integrable with a single solar cell. Precision calorimetry measurements are employed to establish the converter power loss and confirm that an efficiency of 96.2% has been achieved for the 650-mW converter with 20-kHz switching frequency. Finally, both the static and the dynamic tests are conducted to evaluate the tracking performances of the MPPT hardware. The experimental results verify a tracking efficiency higher than 95% under three different insolation levels and a power loss less than 5% of the available cell power under instantaneous step changes between three insolation levels.**

***Key words* – incremental conductance, maximum power point tracking, MPPT, photovoltaic, PV.**

I. INTRODUCTION

With global concerns in regard to the demand, production and price of liquid fuels, the automotive industry has recently seen a major upswing in the hybrid and electric vehicles markets [1]-[4]. It is predicted that 12% of light vehicles sales in 2025 will be hybrids [4]. The hybrid and electric vehicles can significantly benefit from the inclusion of the solar arrays, which can function as the additional energy input or the range extender [3], [5]. In the vehicular applications, however, the limited surface area, the solar array curvature and the rapid insolation changes demand high efficiency photovoltaic cells and highly distributed maximum power tracking arrangements.

Power tracking at the single cell level represents the "end point" for a distributed power tracking architecture and this is made possible by high performance cells such as the Emcore GaAs triple junction cell shown in Fig. 1 [6]. A Maximum Power Point Tracker based on the improved Incremental Conductance (IncCond) method has been previously developed for a single triple junction solar cell for vehicle solar arrays [7], [8].

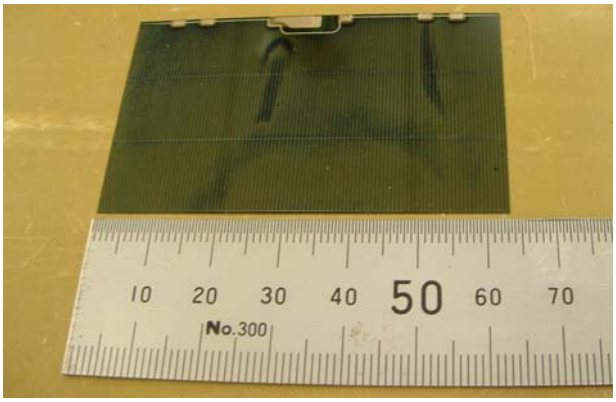

Fig. 1. Emcore GaAs triple junction cell

This paper presents the hardware implementation of the Maximum Power Point Tracker and illustrates that high efficiency and performance can be achieved at a reasonable cost. Significant efforts have been made to achieve a minimized physical size so that the device can be easily integrated with a single photovoltaic (PV) cell. The hardware components are also carefully selected to optimize the total power loss and cost. The converter power loss measured by the calorimetry method confirms that the 650-mW converter is able to achieve an efficiency of 96.2% with a 20-kHz switching frequency. In order to investigate the tracking performance of the proposed Maximum Power Point Tracker, both the static and the dynamic tests are conducted and the experimental results are provided at the end of the paper.

II. MPPT CONTROL METHOD

In the past, many Maximum Power Point Tracking (MPPT) approaches have been developed [9]-[13]. Among these, Hill Climbing or Perturb and Observe (P&O) and IncCond are two popular methods [14]-[17]. These two methods require the measurements of both the cell voltage and current to establish the Maximum Power Point (MPP) under specific environmental conditions. However, as the proposed Maximum Power Point Tracker targets at the single cell level and the power rating falls in the milliwatt range, reducing the cost and the design complexity become overwhelmingly important [18].

An improved IncCond method without the current

sensor has been previously proposed as the MPPT control solution [8]. In this method, the MPP can be established by the cell voltage v_{cell} and the converter switching duty ratio D alone. The MPP equation is:

$$D + v_{cell}\frac{dD}{dv_{cell}} = 0 \tag{1}$$

When $D + v_{cell}\frac{dD}{dv_{cell}} > 0$, the operating point is to the left of the MPP. When $D + v_{cell}\frac{dD}{dv_{cell}} < 0$, the operating point is to the right of the MPP.

Fig. 2 shows the simplified MPPT control block diagram. In Fig. 2, D(j), V_{ref}(j) and v_{cell}(j) are respectively the converter switching duty ratio, the demanded cell voltage and the actual cell voltage in the j^{th} MPPT controller cycle, where j = k, k+1. The MPPT controller calculates the new cell voltage set point based on the converter switching duty ratios and the measured cell voltages in the past and at present. The Proportional-Integral (PI) controller forces the cell voltage to follow the demanded cell voltage signal.

In the practical design of the control software, the threshold ε_j ($j = 1, 2, 3$), which is a small positive number close to zero, is used to determine whether the MPP has been reached and C_V is used as a positive increment in the demanded cell voltage. The variable δ_j ($j = 1, 2, 3$) can be defined as:

$$\delta_1 = v_{cell}(k+1) - v_{cell}(k) \tag{2}$$

$$\delta_2 = D(k+1) - D(k) \tag{3}$$

$$\delta_3 = D(k+1) + v_{cell}(k+1)\frac{\delta_2}{\delta_1} \tag{4}$$

When $|\delta_1| > \varepsilon_1$, the MPPT controller can be simplified as:

$$V_{ref}(k+1) = \begin{cases} V_{ref}(k) + C_V, & \delta_3 > \varepsilon_3 \\ V_{ref}(k), & |\delta_3| < \varepsilon_3 \\ V_{ref}(k) - C_V, & \delta_3 < -\varepsilon_3 \end{cases} \tag{5}$$

When $|\delta_1| < \varepsilon_1$, the MPPT controller can be simplified as:

$$V_{ref}(k+1) = \begin{cases} V_{ref}(k) + C_V, & \delta_2 > \varepsilon_2 \\ V_{ref}(k), & |\delta_2| < \varepsilon_2 \\ V_{ref}(k) - C_V, & \delta_2 < -\varepsilon_2 \end{cases} \tag{6}$$

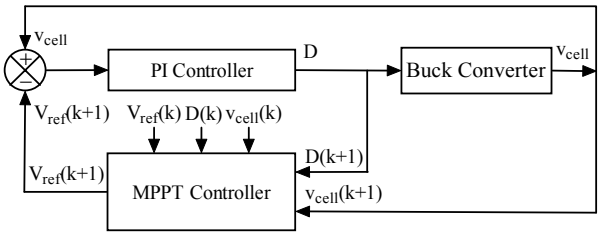

Fig. 2. MPPT control block diagram

In the vehicular applications, the insolation changes much more rapidly than the temperature does. As the cell MPP voltages only vary slightly under different insolation levels, the PI controller runs at a much faster frequency than the MPPT to force the cell voltage to follow the demanded voltage. The MPPT controller executes once every 16 PI control cycles.

It is also worth mentioning that the PI and the MPPT controllers in Fig. 2 are implemented by the Texas Instrument MSP430 microprocessor, which is designed for 1.8-V minimum supply voltage. As the cell voltage may fall below 1.8 V under rapid insolation changes, the switching control signals for the MPPT converter will be suspended by the software once the under voltage happens to allow the cell voltage to recover and the microprocessor to function properly.

III. Hardware Design

Fig. 3 shows the circuit diagram of the MPPT device. The MPPT employs a buck converter topology. This arrangement allows multiple MPPT devices to share a single inductor on the load side and results in a MPPT converter with a possibly more compact inductorless design. The microprocessor is powered directly by one triple junction GaAs solar cell. The gate driver requires a higher voltage and this is achieved by a charge pump circuit made from four Schottky diodes and four capacitors. The key components used in the buck converter are listed as follows.

- Microprocessor – Texas Instrument MSP430F1122IPW, supply voltage 1.8 V to 3.6 V, flash memory 4 KB, RAM 256 B.
- Gate driver – STMicroelectronics TS862ID, supply voltage 2.7 V to 10 V.

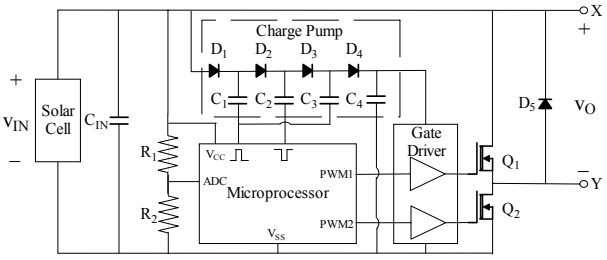

Fig. 3. MPPT device circuit diagram

- Capacitor C_{IN} – AVX surface mount tantalum capacitor TPSC107K006R0150, 100 µF, rated dc voltage 6.3 V, Equivalent Series Resistance (ESR) 150 mΩ, 200-µF capacitance used.
- Diodes D_1 to D_4 – BAS125-07W, $V_{RRM} = 25\ V$, $I_F = 100\ mA$, $V_F = 0.385\ V$, $C_T = 1.1\ pF$.
- MOSFETs Q_1 and Q_2 – International Rectifier IRF7821PBF, $V_{DS} = 30\ V$, $I_D = 13.6\ A$, $R_{DS(on)} = 12.5\ m\Omega$, $Q_g = 14\ nC$.
- Diode D_5 – International Rectifier 10BQ015, $V_{RRM} = 15\ V$, $I_F = 1\ A$, $V_F = 0.35\ V$.

In the hardware implementation of the MPPT device, significant efforts have been made to optimize the size, cost and power loss. Fig. 4 shows the photo of the MPPT hardware. The converter has a size of 18 mm × 21 mm (0.71 in × 0.83 in) and is ready to be integrated with the single solar cell. The total cost of the key components other than the standard surface mount capacitors and resistors in the MPPT hardware shown in Fig. 4 is $5.06 US. A cost breakdown is provided in Table I. The prices shown are based on an order quantity of 10,000 units from three online electric component suppliers including Avnet, Inc., Digi-Key Corporation and Newark InOne [19]-[21]. It is expected that the cost of the standard surface mount components and the Printed Circuit Board (PCB) manufacturing will only be a few percents of the total key components cost under mass production.

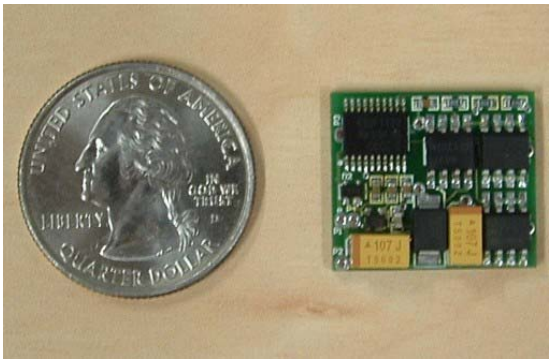

Fig. 4. MPPT hardware

TABLE I
MPPT HARDWARE COST BREAKDOWN

Component	Unit Price (US$)	Number of Components Required	Supplier
MSP430F1122IPW	2.40	1	Avnet
BAS125-07W	0.1432	2	Avnet
10BQ015	0.066	1	Digi-Key
TPSC107K006R0150	0.3432	2	Avnet
IRF7821PBF	0.408	2	Avnet
TS862ID	0.806	1	Digi-Key
Total	5.06	9	-

IV. CALORIMETRY MEASUREMENS

The power loss in the MPPT hardware can be estimated when the converter operates under a switching frequency of 20 kHz and a duty ratio of 50%. The power loss estimations in the key components under a cell supply of 2.275 V and 0.3 A are shown in Table II. The actual total power should be slightly higher than 16.4 mW due to the additional power loss in the charge pump circuit.

Since the total power loss of the MPPT device is only around several percents of the power rating, the determination of the loss will be extremely difficult from the input/output voltage/current measurements. A further complication is that the converter output is inductor free therefore significant switching frequency components will be present in both the output voltage and current waveforms. It is very likely that a significant amount of power is transferred to the R-L load at frequencies other than dc. In this case, calorimetry method provides an indirect power loss measurement and it is much more accurate [22], [23].

The test is conducted inside an environmental chamber, whose temperature controller has an accuracy of ±0.2°C. A Wheatstone bridge consisting of four platinum sensing resistors, Pt100 [24], is used to transform the differential temperature of the system under test and the ambient to the voltage measurement. One voltage reading is logged every 15 minutes by the National Instrument LabVIEW system. Fig. 5 shows the calibration curve in the calorimetry measurement, where the horizontal axis P_{loss} is the power dissipation in the system under test and the vertical axis V_T is the voltage representing the differential temperature. The calibration curve is obtained through the power dissipation of 1-kΩ resistor with 1% tolerance. Under the individual power levels, a settling time of 24 hours is adhered and 12 data representing the differential temperatures over the last three-hour duration are used in the plot. Error bars at the individual measuring points are also shown in Fig. 5 and a maximum differential temperature measurement variation of 16 mV has been observed.

Finally the measured converter power loss is 24.6 mW at an input power of 652 mW and this compares favourably with the total power loss estimation shown in Table II. The measurement confirms that the MPPT converter has achieved an efficiency of 96.2%.

TABLE II
MPPT HARDWARE POWER LOSS ESTIMATION

Item	Power Loss (mW)
Microprocessor	0.7
Capacitor C_{IN} Conduction	6.8
MOSFETs Q_1 and Q_2 Conduction	4.5
MOSFETs Q_1 and Q_2 Gate Drive	3.5
Diode D_5 Conduction	0.9
Total	16.4

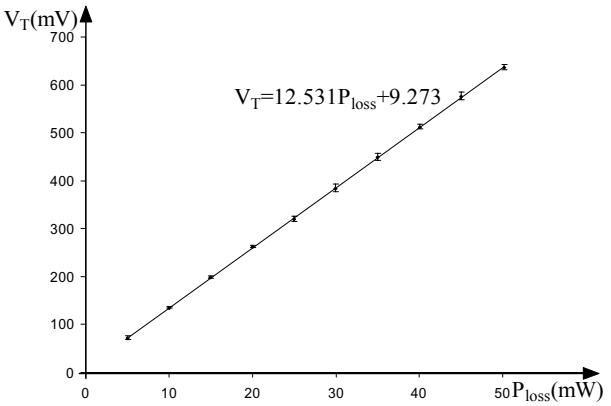

Fig. 5. Calorimetry calibration curve

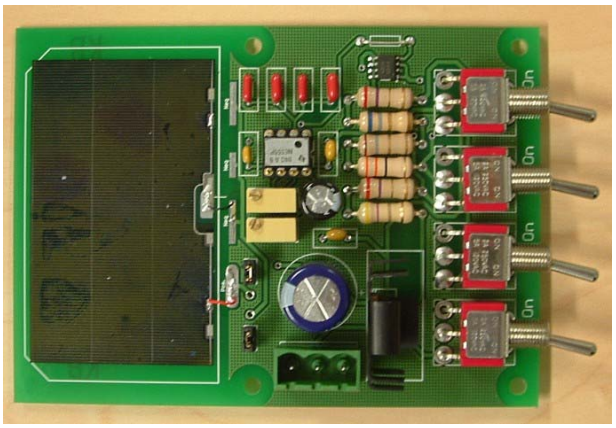

Fig. 6. Solar simulator with an Emcore cell

V. Experimental Results

In order to verify the tracking performance of the MPPT hardware, a solar cell simulator with an Emcore triple junction cell has been built as shown in Fig. 6. In the solar cell simulator, a switchable current source functions as the light-generated current. This current is then injected into the semiconductor junction of the actual solar cell to reproduce its I-V characteristic. The amount of the injected current can be controlled both manually by the mechanical toggle switches and automatically by the combination of a LM555 timer and two MOSFETs.

The I-V and P-V characteristics of the solar cell simulator are obtained through the capacitance load test, in which a capacitor is charged from the short circuit condition to the open circuit condition. The capacitor voltage and current waveforms during the entire process are first captured by a digital oscilloscope. Then the recorded voltage and current data series are transformed to the cell characteristic curves shown in Figs. 7 and 8. In Figs. 7 and 8, the dashed-dotted lines represent the solar cell simulator curves under 1 sun, the solid lines represent those under 0.5 sun and the dashed lines represent those under 0.1 sun. The cell voltage, current and power at the MPPs obtained from Figs. 7 and 8 under three insolation levels are given in Table III.

The static test is conducted to obtain the tracking efficiencies of the MPPT hardware under various steady insolation levels. In the static test, the cell voltage, current and power are measured under the three individual insolation levels and the results are shown in Table IV. It can be seen that the actual cell output powers under 1, 0.5 and 0.1 sun are respectively 98.5%, 97.1% and 95.7% of the corresponding maximum available cell powers given in Table III. The tracking efficiency is lower at 0.1 sun insolation level than that at 1 sun insolation level as the maximum available cell power at MPP under 0.1 sun is extremely low, which is only 8% of that under 1 sun.

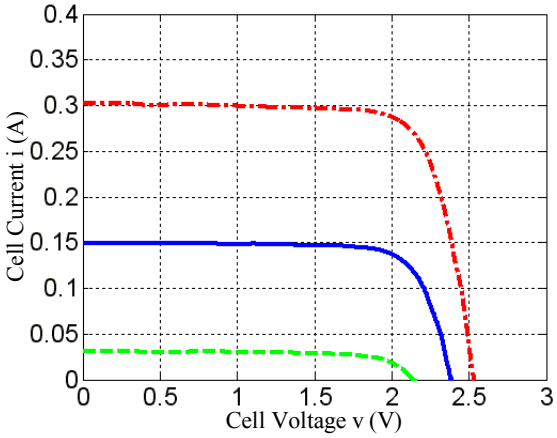

Fig. 7. Solar cell simulator I-V curve

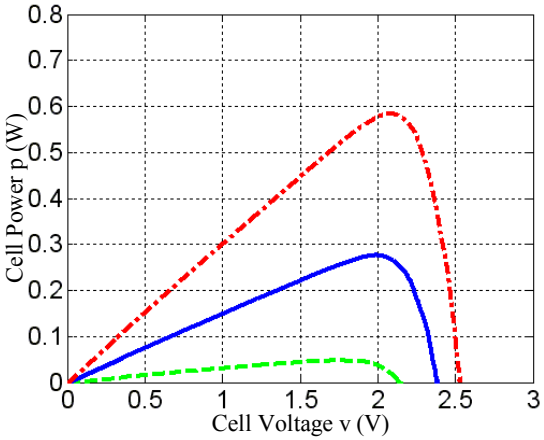

Fig. 8. Solar cell simulator P-V curve

TABLE III
Solar Simulator MPPs under Three Insolation Levels

Insolation	Voltage (V)	Current (A)	Power (W)
1 Sun	2.087	0.280	0.584
0.5 Sun	1.986	0.139	0.276
0.1 Sun	1.766	0.027	0.047

TABLE IV
MPPS UNDER THREE INSOLATION LEVELS OBTAINED BY THE MPPT HARDWARE

Insolation	Voltage (V)	Current (A)	Power (W)	Tracking Efficiency
1 Sun	1.966	0.293	0.575	98.5%
0.5 Sun	1.879	0.143	0.268	97.1%
0.1 Sun	1.718	0.026	0.045	95.7%

The dynamic test studies the MPPT hardware transient tracking performances in motion under the influence of the roadside objects. Specific conditions are created where the insolation is subject to instantaneous step changes between full and partial sun of 50-ms duration each and this simulates the situation where the vehicle mounted cells travel at 20 ms^{-1} through joining light and shadow sections of 1 meter wide each. The cell power waveforms are recorded so that the tracking power losses can be duly calculated.

The waveforms of the power when the insolation is under instantaneous step changes between 1 and 0.5 sun are shown in Figs. 9 and 10, where the solid, the dashed and the dashed-dotted lines respectively represent the actual, the maximum available and 90% of the maximum available powers. It can be seen that the actual cell powers are largely controlled to be higher than 90% of the maximum available cell powers under both insolation step up and step down.

The same set of power waveforms when the insolation is under instantaneous step changes between 1 and 0.1 sun are shown in Figs. 11 and 12. As shown in Fig. 11, when the insolation steps down instantaneously from 1 to 0.1 sun, the cell voltage initially drops below 1.8 V between 10 ms and 26 ms and this causes the converter to shut down. As shown in Fig. 12, the actual cell power drops to about 35% of the maximum available cell power when the insolation steps up instantaneously from 0.1 to 1 sun. The establishment of the new MPPs also takes a much longer time than those under insolation instantaneous step changes between 1 and 0.5 sun. The much inferior performances are caused by a much greater difference between insolation levels and a much longer response time of the PI controller.

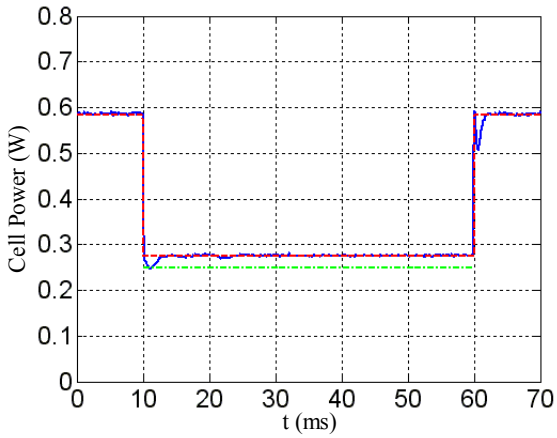

Fig. 9. Cell power in 1-m shadow section (1 to 0.5 sun)

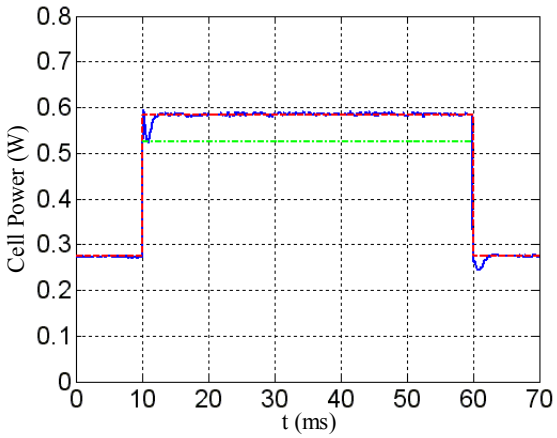

Fig. 10. Cell power in 1-m li ght section (0.5 to 1 sun)

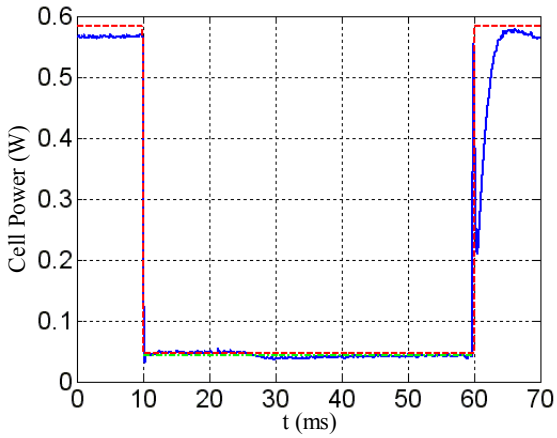

Fig. 11. Cell power in 1-m shadow section (1 to 0.1 sun)

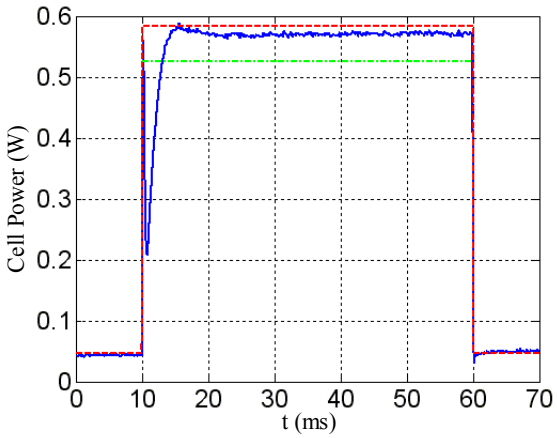

Fig. 12. Cell power in 1-m light section (0.1 to 1 sun)

TABLE V
MPPT HARDWARE LOSSES UNDER INSTANTANEOUS INSOLATION STEP CHANGES

Insolation Step Change Condition		Between 1 and 0.5 sun	Between 1 and 0.1 sun
Energy Loss	Insolation Step Up (mJ)	0.044	1.287
	Insolation Step Down (mJ)	0.017	0.051
Average Available Maximum Cell Power (mW)		430	315.5
Power Loss	Absolute (mW)	0.6	13.4
	Percentage (%)	0.14	4.25

The loss calculations in the dynamic tests are shown in Table V. The MPPT hardware has a very low power loss of 0.14% when the insolation levels step up and down between 1 and 0.5 sun. Due to the significant change of the insolation levels between 1 and 0.1 sun, the average power loss is 4.25%, which is much higher than the first case. However, this is unlikely to be disastrous.

VI. CONCLUSIONS

This paper studies the hardware implementation of a Maximum Power Point Tracker which is based on IncCond MPPT method without the current sensor. The MPPT hardware has achieved a size of 18 mm × 21 mm (0.71 in × 0.83 in) and a cost to close to $5 US. The minimized size and cost opens the opportunity for the fabrication of solar cells with the embedded MPPT controller to drive the cost down in the installation process. High conversion efficiency and tracking performances are also achieved by the prototype MPPT device. Calorimetry measurements have confirmed that the 650-mW converter switching at 20 kHz has an overall efficiency of 96.2%. The experimental results of both the static and the dynamic tests have verified a minimum steady-state tracking efficiency of 95.7% and a maximum dynamic power loss of 4.3% under the set conditions.

ACKNOLEDGEMENT

This work was supported by the Queensland Department of Public Works and Housing and the Queensland Department of Transport.

REFERENCES

[1] J. Voelcker, "Top 10 tech cars, here come the hybrids," *IEEE Spectr.*, Vol. 41, No. 3, pp. 20-27, Mar. 2004.
[2] J. Voelcker, "Top 10 tech cars, a year of stability," *IEEE Spectr.*, Vol. 42, No. 3, pp. 16-24, Mar. 2005.
[3] J. Voelcker, "Top 10 tech cars, hybrids square off against diesels for the economy laurels," *IEEE Spectr.*, Vol. 43, No. 4, pp. 24-33, Apr. 2006.
[4] J. Voelcker, "Top 10 tech cars 2007, electric cars are back," *IEEE Spectr.*, Vol. 44, No. 4, pp. 34-41, Apr. 2007.
[5] A. Simpson, G. Walker, M. Greaves, D. Finn and B. Guymer, "The ultra commuter: a viable and desirable solar powered commuter vehicle," in *Proc. Australasian Universities Power Engineering Conference*, 2002.
[6] Emcore Corporation. InGaP/GaAs/Ge triple-junction solar cells. [Online]. Available: http://www.emcore.com/assets/photovoltaics/Triple.pdf
[7] P. Wolfs and L. Tang, "A single cell maximum power point tracking converter without a current sensor for high performance vehicle solar arrays," in *Proc. IEEE PESC*, 2005, pp. 165-171.
[8] P. Wolfs and Q. Li, "A current-sensor-free incremental conductance single cell MPPT for high performance vehicle solar arrays," in *Proc. IEEE PESC*, 2006, pp. 117-123.
[9] C. Hua and C. Shen, "Comparative study of peak power tracking techniques for solar storage system," in *Proc. IEEE APEC*, 1998, pp. 679-685.
[10] C. Hua and C. Shen, "Study of maximum power tracking techniques and control of dc/dc converters for photovoltaic power system," in *Proc. IEEE PESC*, 1998, pp. 86-93.
[11] D. P. Hohm and M. E. Ropp, "Comparative study of maximum power point tracking algorithms using an experimental, programmable, maximum power point tracking test bed," in *Proc. IEEE PSC*, 2000, pp. 1699-1702.
[12] T. Esram, J. W. Kimball, P. T. Krein, P. L. Chapman and P. Midya, "Dynamic Maximum Power Point Tracking of Photovoltaic Arrays Using Ripple Correlation Control," *IEEE Trans. Power Electron.*, Vol. 21, No. 5, pp. 1282-1291, Sept. 2006.
[13] T. Esram and P. L. Chapman, "Comparison of photovoltaic array maximum power point tracking techniques," *IEEE Trans. Energy Conversion*, in press.
[14] A. F. Boehringer, "Self-adapting dc converter for solar spacecraft power supply," *IEEE Trans. Aerosp. Electron. Syst.*, Vol. AES-4, No. 1, pp. 101-111, Jan. 1968.
[15] O. Wasynczuk, "Dynamic behavior of a class of photovoltaic power systems," *IEEE Trans. Power App. Syst.*, Vol. 102, No. 9, pp. 3031-3037, Sept. 1983.
[16] B. K. Bose, P. M. Szczesny, and R. L. Steigerwald, "Microcomputer control of a residential power conditioning system," *IEEE Trans. Ind. Applicat.*, Vol. 21, No. 5, pp. 1182-1191, Sept./Oct. 1985.
[17] K. H. Hussein, I. Muta, T. Hoshino and M. Osakada, "Maximum photovoltaic power tracking: an algorithm for rapidly changing atmospheric conditions," in *IEE Proc. Generation, Transmission and Distribution*, Vol. 142, No. 1, pp. 59-64, Jan. 1995.
[18] A. Pandey, N. Dasgupta and A. K. Mukerjee, "A simple single-sensor MPPT solution," *IEEE Trans. Power Electron.*, Vol. 22, No. 2, pp. 698-700, Mar. 2007.
[19] Avnet, Inc. [Online]. Available: https://www.em.avnet.com
[20] Digi-Key Corporation. [Online]. Available: http://www.digikey.com
[21] Newark InOne. [Online]. Available: http://www.newark.com
[22] D. Patterson, "Simple calorimetry for accurate loss measurement," *IEEE Power Electronic Society Newsletter,* pp. 5-7, Oct. 2000.
[23] P. D. Malliband, N. P. van der Duijn Schouten and R. A. McMahon, "Precision calorimetry for the accurate measurement of inverter losses," in *Proc. IEEE PEDS*, 2003, pp. 321-326.
[24] Labfacility LTD. Pt100 Datasheet. [Online]. Available: http://www.temperature-sensors1.com/pdf/sensors-PRTs.pdf